Chemical Engineering Journal 458 (2023) 141445

Contents lists available at ScienceDirect

Chemical Engineering Journal

journal homepage: www.elsevier.com/locate/cej

Synergistic enhancement of Li-S battery low-temperature cycling performance by nano-sized uniformly compounded FeCoNi and MnO nanoparticles

Xiaowan Pang [a,b], Baigang An [a,*], Shumin Zheng [b,*], Bao Wang [b,*]

[a] School of Chemical Engineering, University of Science and Technology Liaoning, 185 Qianshanzhong Road, Anshan 114051, China
[b] State Key Laboratory of Biochemical Engineering, Institute of Process Engineering, Chinese Academy of Sciences, Beijing 100190, China

ARTICLE INFO

Keywords:
Low temperature
Li-S battery
Medium entropy alloy
FeCoNi nanoparticles
MnO nanoparticles

ABSTRACT

Lithium-sulfur (Li-S) battery has high energy density, which demonstrated the potential to conquer the energy storage market. However, in cryogenic circumstances, due to polysulfides (LiPSs) clustering, slow electrochemical reaction, and serious polarization, commercial applications are seriously hindered. Previous works proved that alloy particles enable high-performance low-temperature Li-S batteries, nevertheless, the cycling stability is unsatisfactory due to the serious shuttle effect at low temperatures. Here, FeCoNi nanoparticles (NPs) were introduced as a catalyzer, benefiting from the structural and compositional merits it can synergistically catalyze more kinds of LiPSs. To enhance adsorption ability, MnO NPs were used to anchor LiPSs, thus providing a higher concentration of LiPSs around FeCoNi NPs and MnO NPs, thereby preventing the shuttle effect and enhancing cycling stability at low temperatures. Finally, a composite cathode material FCN-MO@CNFs was synthesized by one-step in-situ pyrolysis. Via detailed electrochemical analysis, FCN-MO@CNFs exhibited excellent electrocatalytic activity and achieved satisfactory low-temperature cycling performance. The initial discharge capacity reaches 1167.5 mAh g^{-1} under −40 °C at 0.1C, and the capacity retention rate reaches 70.1 % after 100 cycles at 0.2C. This work provides a novel method for the practical development of high-performance low-temperature Li-S batteries.

1. Introduction

To provide power for our increasingly electrified society, energy storage technology must be developed to meet the growing demand, and energy storage equipment must meet the requirements of safe and reliable operation in a variety of climates. The widespread adoption of electric vehicles is challenged by the short-range at low temperatures, which is due to the sharply diminished capacity and power output of commercial Li-ion batteries [1]. In addition, when applications are associated with military, aviation, and navigation, batteries need to operate in extreme environments where the temperatures are far below 0 °C [2]. However, the low-temperature operation is a great challenge for batteries, due to the low charge/discharge capacity [3]. Advanced batteries with high energy density may become the most promising candidate at low temperatures.

Li-S battery is regarded as one of the most promising storage systems owing to its high theoretical capacity and energy density [4–8]. However, the Li-S battery has a high Li-ion desolvation energy barrier at low temperatures, which leads to the increase of charge transfer resistance [9], strong battery polarization [10], and the decrease of Li_2S_x solubility, which not only promotes the formation of strong clusters but also passivates the cathode [11,12], making it difficult to achieve full charge/discharge. Further, the shuttle effect of LiPSs leads to capacity fade. These problems become more serious with the decreased temperature, which hinders the application of Li-S batteries in cryogenic climates.

Up to now, there are few studies reporting on low-temperature charge/discharge of Li-S batteries [13–18]. Strategies for improving low-temperature performance mainly include the development of novel electrolytes [10,11], the designing of cathode materials [13,15], and the functionalization of separators [19–21]. We improve low-temperature performance from the perspective of the cathode. Wang et al. prepared Co_3S_4@carbon nanotube(CNT)-S cathode, the initial discharge capacity of the composite cathode is 1275.6 mAh g^{-1} under −25 °C

* Corresponding authors.
E-mail addresses: bgan@ustl.edu.cn (B. An), smzheng@ipe.ac.cn (S. Zheng), baowang@ipe.ac.cn (B. Wang).

https://doi.org/10.1016/j.cej.2023.141445
Received 7 November 2022; Received in revised form 27 December 2022; Accepted 11 January 2023
Available online 13 January 2023

benefit from the adsorption and catalysis effect of Co_3S_4 on LiPSs and the high conductivity of CNTs [22]. Gao et al. synthesized CoFe@C@CNFs as the sulfur host for Li-S battery, the composite materials possess a high affinity for LiPSs and can accelerate the catalytic conversion process, it has a specific capacity of 836 mAh g^{-1} under −20 °C at 0.2C [23].

Driven by these studies, we developed a high-performance composite cathode material (FeCoNi@CNFs) consisting of FeCoNi entropy alloy nanoparticles and carbon nanofibers (CNFs) in our previous work [24]. As the sulfur host for Li-S battery, it has ultra-high specific capacity at low temperatures. Unfortunately, its capacity retention at low temperatures is not ideal. This is also verified by the previous literature, which reported that alloy NPs can achieve high-performance low-temperature Li-S batteries, but their capacity is significantly reduced due to the shuttle effect [23]. Therefore, to solve the problem of large fade of capacity at low temperatures, the addition of metal oxides is of great significance to prevent the shuttle effect and enhance the physical and chemical adsorption of LiPSs.

Herein, we introduced MnO NPs into FeCoNi@CNFs via one-step in-situ pyrolysis. In H_2, Fe^{3+}, Ni^{2+}, and Co^{2+} are all reduced to simple substances, forming alloy due to similar chemical bond properties, while Mn^{2+} is reduced to MnO [25]. Finally, a new composite cathode material FCN-MO@CNFs is formed. Atomic scale mixed medium entropy alloy FeCoNi NPs have high catalytic activity and good adsorption, which can synergistically catalyze the conversion of LiPSs and speed up the electrochemical reaction. The addition of MnO NPs can anchor and increase the concentration of LiPSs around FeCoNi NPs, realize strong adsorption of LiPSs, improve the utilization rate of active materials, Promote catalytic conversion of LiPSs, and prevent the shuttle effect. CNFs with unique three-dimensional porous network structure have a large specific surface area, excellent conductivity, and electrolyte wettability, which can effectively prevent the accumulation of LiPSs and avoid volume expansion. The composite cathode material enhances the catalytic conversion ability of LiPSs at low temperatures, accelerating the reaction progress and improving the low-temperature cycling stability. By systematically investigating the rate cycling performance of the batteries at 30 °C, −10 °C, and −40 °C, it is verified that FCN-MO@CNFs has excellent battery performance at a wide temperature range. The initial discharge capacity can reach 1167.5 mAh g^{-1} under

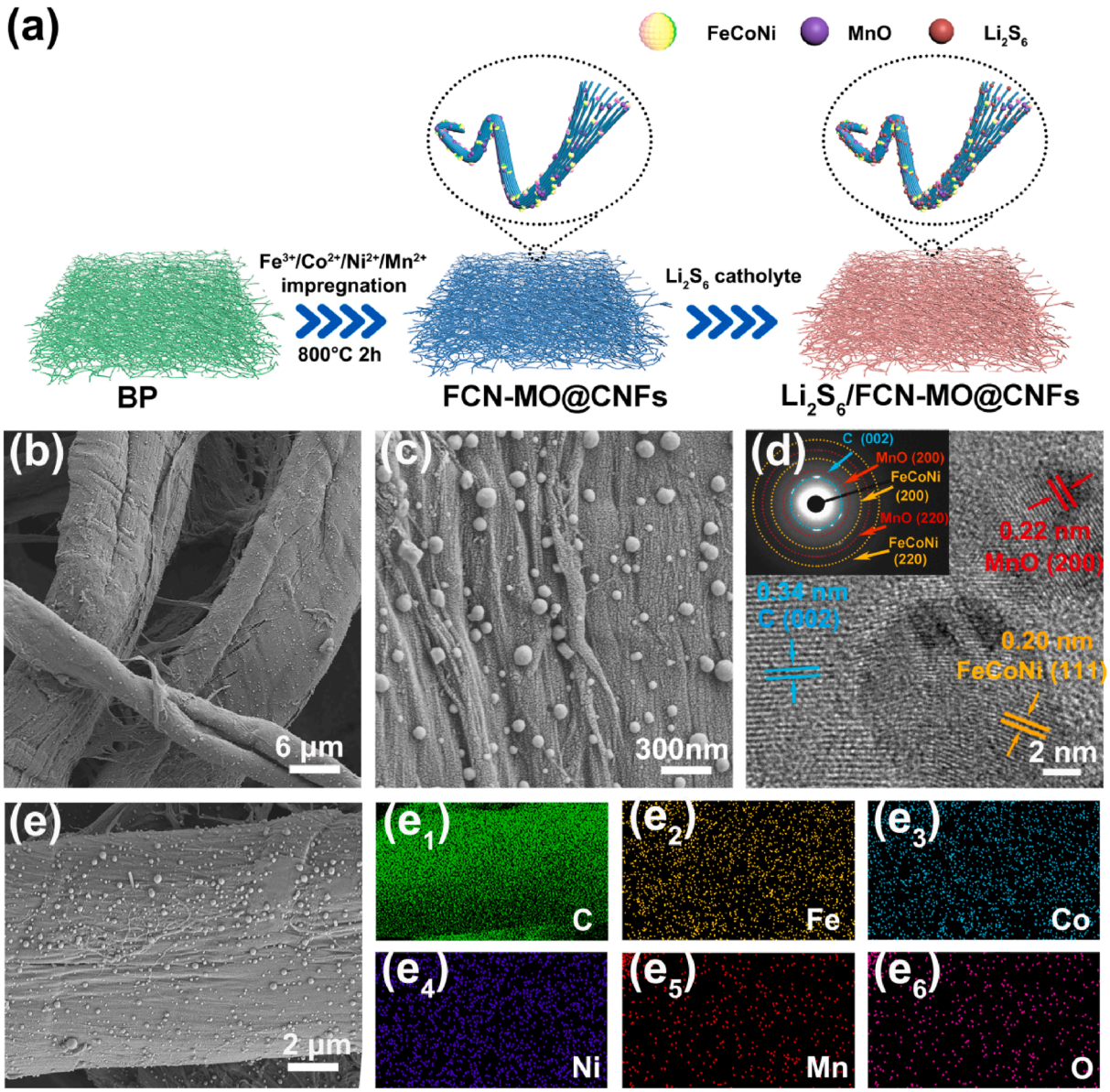

Fig. 1. (a) The synthesis process of Li_2S_6/FCN-MO@CNFs. (b-c) SEM images of FCN-MO@CNFs. (d) HRTEM image with SAED pattern. (e) Corresponding elemental mapping images of FCN-MO@CNFs.

−40 °C at 0.1C, and the capacity retention rate can reach 70.1 % after 100 cycles at 0.2C.

2. Results and discussion

The synthesis procedure of Li_2S_6/FCN-MO@CNFs is demonstrated in Fig. 1a, and a detailed method is given in the experimental section. We used trans blot filter paper (BP), $FeCl_3{\cdot}6H_2O$, $CoCl_2{\cdot}6H_2O$, $NiCl_2{\cdot}6H_2O$, and $MnCl_2{\cdot}4H_2O$ as raw materials to prepare Li_2S_6/FCN-MO@CNFs via relatively simple immersion, heat treatment, and Li_2S_6 dropping. When the temperature was maintained at 800 °C, the added Fe^{3+}, $Ni^{2+,}$ and Co^{2+} form FeCoNi alloy NPs due to their similar chemical bond properties, while the Mn^{2+} has strong reducibility and is conducive to phase dispersion. Therefore, it is reduced to MnO NPs under Ar-H_2 and uniformly dispersed on CNFs [25]. In addition, we set up a control group that did not add metal salt solution to the BP.

To visually observe the surface morphology and microstructure of FCN-MO@CNFs, the synthetic materials were tested by scanning electron microscopy (SEM) and transmission electron microscopy (TEM). It is apparent from Fig. 1b, c and Fig. S1 that FCN-MO@CNFs is a three-dimensional porous structure, and CNFs are twisted in the form of hemp rope, with an average diameter of about 10 μm. FeCoNi and MnO NPs are uniformly dispersed in CNFs. The electrolyte permeability test shows that the electrolyte can soaks the material very quickly with a speed of 0.1 s. This shows that this unique structure enhances the contact between the active substance and the electrolyte (Fig. S2, Video S1). The high-resolution TEM (HRTEM) image (Fig. 1d) presents three distinct fringes with spacings of 0.20, 0.34, and 0.22 nm, respectively, corresponding to FeCoNi (111), C (002), and MnO (200) facets. Selected area electron diffraction (SAED) patterns in Fig. 1d confirmed the existence of FeCoNi alloy and MnO NPs. EDS mapping images (Fig. 1e) show that Fe, Co, and Ni elements are highly dispersed, and Mn and O elements are also uniformly dispersed on CNFs.

The X-ray diffraction (XRD) patterns of FCN-MO@CNFs show three peaks at 44.2°, 51.5°, and 75.7°, corresponding to (111) (200) (220) planes (COD ID 9000089) of FeCoNi alloy, and three peaks at 35.1°, 40.8°, and 59.0°, corresponding to (111) (200) (220) crystal plane (ICOD ID 0750625) of MnO. The 26.6° peak corresponds to the (002) plane of graphite carbon (Fig. 2a and Fig. S3), this is consistent with the TEM results. The porous structures of FCN-MO@CNFs was investigated by the N_2 adsorption–desorption measurements. FCN-MO@CNFs shows hierarchical microporous and mesoporous structures, which is conducive to the adsorption and conversion of LiPSs. The larger specific surface area allows the material to maximize its contact with LiPSs.

The high-resolution X-ray photoelectron spectroscopy (XPS) Mn 2p spectra reveal that Mn $2p_{3/2}$ and Mn $2p_{1/2}$ peaks have binding energy positions of 641.2 eV and 653.1 eV, which is consistent with the Mn 2p spectra of MnO (Fig. 2c) [26]. In the Fe 2p, Co 2p, and Ni 2p spectra (Fig. 2d, e), there are Fe^0, $Co^{0,}$ and Ni^0 peaks, which determine the formation of FeCoNi alloys. The C 1 s spectrum reflects the different structures of carbon in FCN-MO@CNFs. (Fig. S4).

To verify the adsorption effect of LiPSs on FCN-MO@CNFs, CNFs (B) and FCN-MO@CNFs (C) were independently added to Li_2S_6 (A) solution and carried out a visual adsorption experiment, Fig. 3a. After the solution was allowed to stand for 3 h, the color of Li_2S_6 solution added to FCN-MO@CNFs was close to light yellow, while in CNFs, no significant change occurred, which further indicated that FCN-MO@CNFs had excellent chemical anchoring ability to LiPSs. In Fig. 3b, electrochemical impedance spectroscopy (EIS) shows that Li_2S_6/FCN-MO@CNFs has a low charge transfer resistance, which indicates that FCN-MO can accelerate ion/electron transfer, which is conducive to the redox reaction of LiPSs.

The electrochemical characteristics of the electrodes were further examined by cyclic voltammetry (CV). In Fig. 3c, two pairs of redox peaks can be identified, in which A-A' pair corresponds to the redox reaction between S_8 and LiPSs, and B-B' pair corresponds to the redox reaction between LiPSs and LiS_2. Fig. 3d shows the constant current charge/discharge curves of Li_2S_6/CNFs and Li_2S_6/FCN-MO@CNFs cathodes in the first cycle at a constant current rate of 0.1C in the range of 1.7 V-2.8 V. Comparing with Li_2S_6/CNFs (ΔE = 190 mV), Li_2S_6/FCN-MO@CNFs cathode shows smaller potential polarization (ΔE = 130 mV), which proves that FCN-MO@CNFs is beneficial to the redox reaction process of Li-S battery. Constant current charge/discharge tests were conducted under different current densities to determine the rate performance of cathodes. In Fig. 3e, the rate performance of Li_2S_6/Sample 2 is significantly higher than that of other samples. Further,

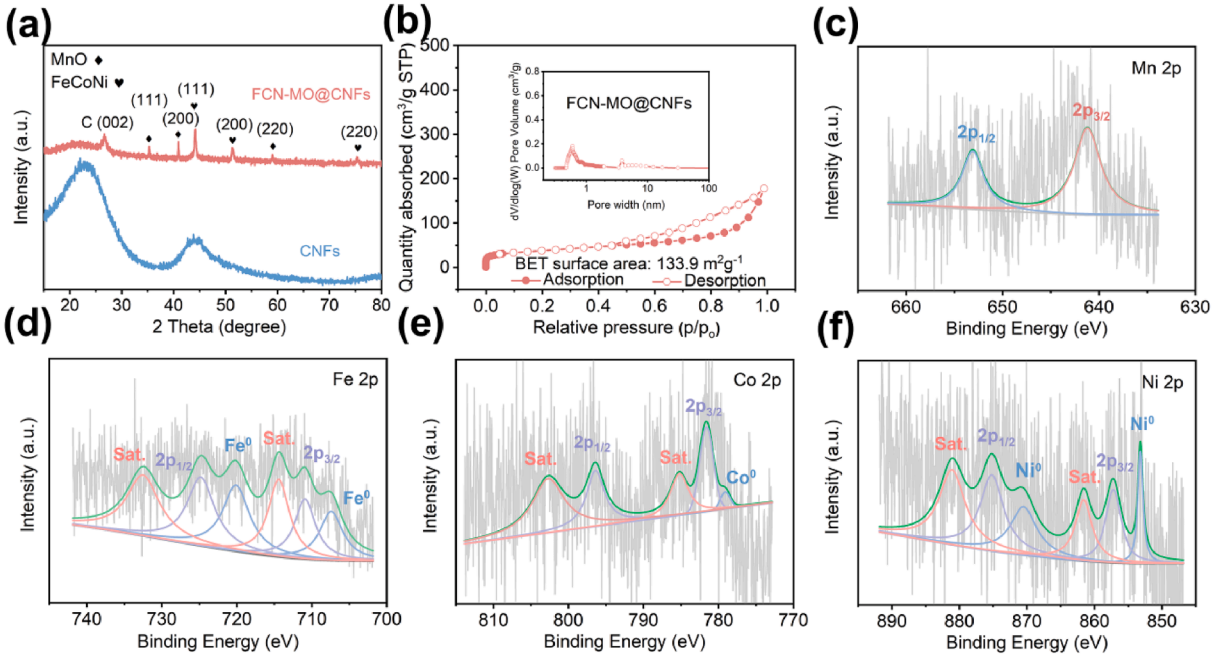

Fig. 2. (a) XRD patterns of CNFs and FCN-MO@CNFs. (b) Nitrogen adsorption/desorption isotherms of FCN-MO@CNFs. Inset: pore size distribution of the material. (c-f) Mn 2p, Fe 2p, Co 2p, and Ni 2p XPS spectra of FCN-MO@CNFs.

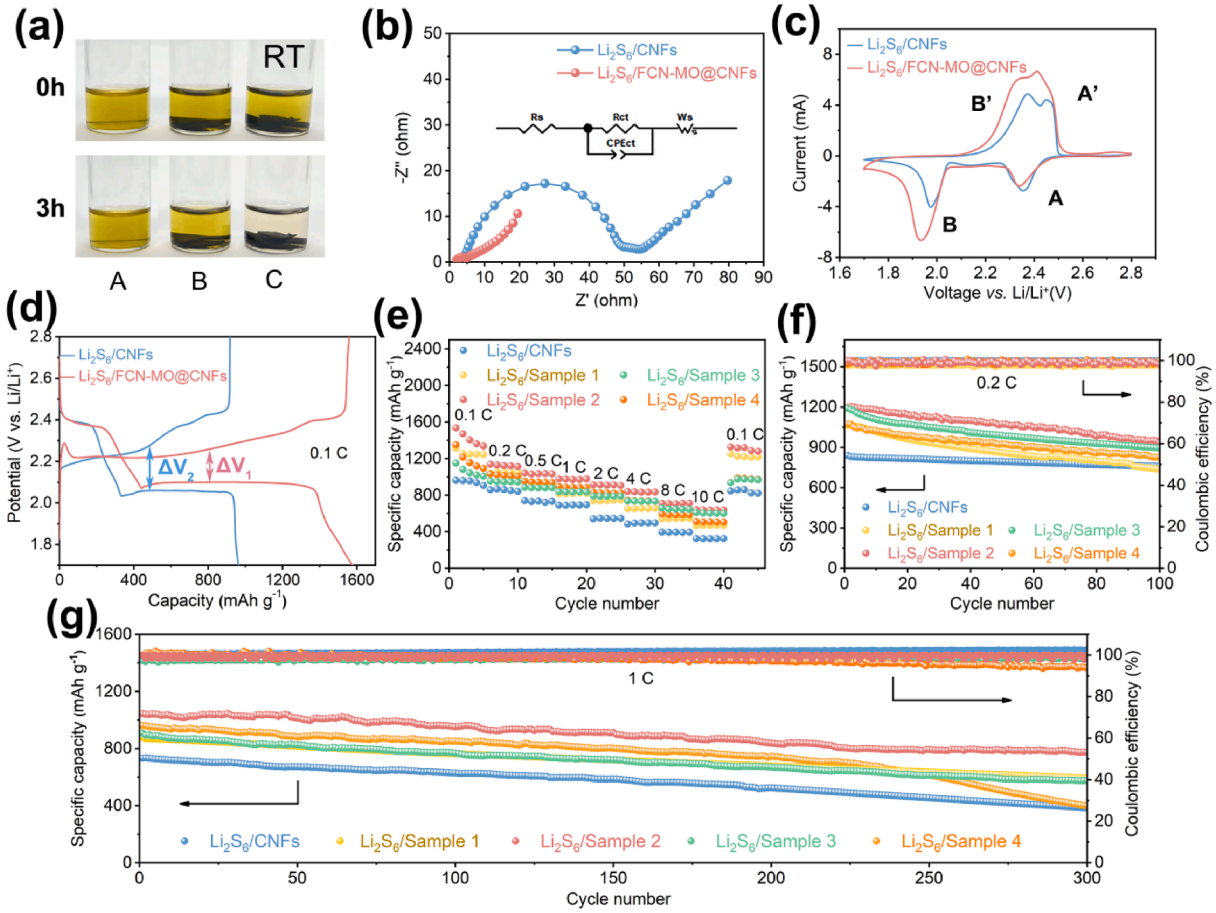

Fig. 3. (a) Optical image of L_2S_6 adsorption tests by CNFs and FCN-MO@CNFs after 3 h under room temperature. (b) EIS plots of Li_2S_6/CNFs and Li_2S_6/FCN-MO@CNFs. Inset: corresponding equivalent circuit model. (c) CV curves of Li_2S_6/CNFs and Li_2S_6/FCN-MO@CNFs at a scan rate of 0.4 mV s^{-1}. (d) Constant-current discharge/charge curves of Li_2S_6/CNFs and Li_2S_6/FCN-MO@CNFs. (e) Rate performance of Li_2S_6/CNFs and Li_2S_6 of samples. Cycling performance of Li_2S_6/CNFs and Li_2S_6 of samples at (f) 0.2C and (g) 1C. All tests were performed at room temperature (RT).

compared with other materials, Li_2S_6/Sample 2 shows the high initial capacity and cycle stability at 0.2C and 1C (Fig. 3f, g). The capacity retention rate is 80.0 % after 100 cycles at 0.2C and 74.1 % after 300 cycles at 1C.

We selected Li_2S_6/Sample 2, which has the best performance at room temperature, to explore the battery performance at low temperatures, and labeled it as Li_2S_6/FCN-MO@CNFs. The rate performance of Li_2S_6/FCN-MO@CNFs cathode at −10 °C and −40 °C was evaluated at different current densities of 0.1C, 0.2C, 0.5C, 1C, 2C, 4C, 8C and 10C (Fig. 4a). At −10 °C, its discharge capacity can reach 1250.2, 940.0, 830.1, 726.1, 563.7, 356.8, 288.9, and 278.7 mAh g^{-1}, respectively. At − 40 °C, the corresponding discharge capacity can reach 1167.5, 639.2, 472.7, 409.2, 329.2, 209.7, 108.0, and 17.4 mAh g^{-1}, respectively. After 100 cycles under −10 °C at 0.2C, the capacity retention rate can reach 90.5 % (Fig. 4b). When the temperature drops to −40 °C, the capacity retention rate is 70.1 %. Compared with the capacity retention rate of the ternary alloy cathode material under −40 °C at 0.2C of the previous work, the addition of MnO NPs is more beneficial to the adsorption and catalytic conversion of LiPSs, which greatly improves the stability of the battery. After 210cycles under −10 °C at 1C, the capacity retention rate of Li_2S_6/FCN-MO@CNFs is 85 %; after 210cycles under −40 °C at 1C, the capacity retention rate of Li_2S_6/FCN-MO@CNFs is 18 % (Fig. 4d).

To further explore the role of −40 °C FCN-MO@CNFs in the oxidation and reduction process of LiPSs, we compared the cyclic voltammetry curves of symmetrical batteries with different cathode materials. As shown in Fig. 4e, Li_2S_6/FCN-MO@CNFs has a higher redox peak, which indicates that FCN-MO@CNFs has superior catalytic reaction kinetics. The impedance spectrum at low temperature shows that FCN-MO@CNFs still has low charge transfer resistance, which is conducive to the redox reaction (Fig. 4f). In Fig. 4g, two pairs of redox peaks can still be observed on the cyclic voltammetry curve, indicating that the redox reaction can still occur at low temperatures.

In addition, to explore the adsorption of FCN-MO@CNFs on LiPSs at low temperatures, visualization experiments were performed (Fig. 4c). In the −40 °C low-temperature cabinet, after standing for 5 h, the color of CNFs (B) added with Li_2S_6 (A) solution is slightly darker, while FCN-MO@CNFs (C) is colorless, which indicates that FCN-MO@CNFs has strong adsorption effect on LiPSs. At the same time, we found that Li_2S_6 solution would accumulate at low temperatures, while CNFs added Li_2S_6 solution did not. This also indicates that the unique three-dimensional porous structure of CNFs can prevent the accumulation of LiPSs. Therefore, FCN-MO@CNFs acts out robust adsorption.

3. Conclusions

In this study, we successfully prepared a cathode material for Li-S batteries, which is composed of FeCoNi medium entropy alloy NPs, MnO NPs, and CNFs. The multi-metal synergetic catalysis between FeCoNi alloy NPs produces excellent electrocatalytic activity and promotes redox reaction kinetics. MnO NPs are beneficial to the adsorption of LiPSs, inhibit the shuttle effect of LiPSs, and improve cycle stability. After detailed electrochemical tests, when the concentration of added metal ions is 40 mM, the battery shows excellent cycle and rate performance. Even under −40 °C at 0.1C, the initial discharge capacity

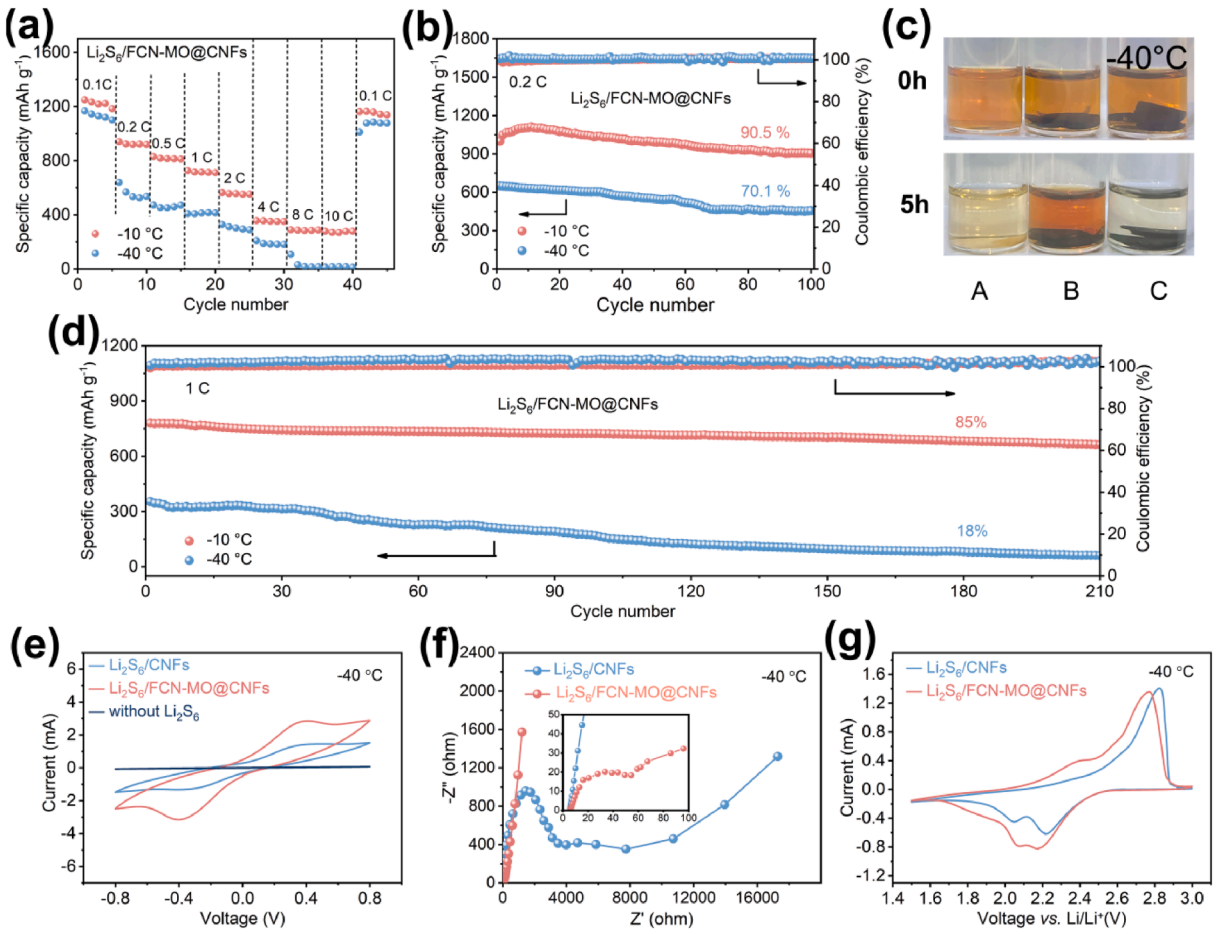

Fig. 4. (a) Rate performance of Li_2S_6/FCN-MO@CNFs under different temperatures. (b) Cycling performance of Li_2S_6/FCN-MO@CNFs at 0.2C under different temperatures. (c) Optical image of L_2S_6 adsorption tests by CNFs and FCN-MO@CNFs after 5 h under −40 °C. (d) Cycling performance of Li_2S_6/FCN-MO@CNFs at 1C under different temperatures. (e) Under −40 °C, CV curves of Li_2S_6/CNFs and Li_2S_6/FCN-MO@CNFs symmetric cells. (f) Under −40 °C, Nyquist plots of Li_2S_6/CNFs and Li_2S_6/FCN-MO@CNFs. (g) Under −40 °C, CV curves of Li_2S_6/CNFs and Li_2S_6/FCN-MO@CNFs at a scan rate of 0.4 mV s^{-1}.

reaches 1167.5 mAh g^{-1}; At 0.2C, the capacity retention rate still reached 70.1 % after 100 cycles. This work provides a simple method for the design of high-performance low-temperature Li-S batteries and has certain enlightenment significance for the future commercial prospects of low-temperature Li-S batteries.

4. Experiment

4.1. Preparation of FCN-MO@CNFs

Dissolve the equivalent amount of $FeCl_3{\cdot}6H_2O$, $CoCl_2{\cdot}6H_2O$, $NiCl_2{\cdot}6H_2O$, and $MnCl_2{\cdot}4H_2O$ in 30 ml deionized water to obtain Fe^{3+}/Co^{2+}/Ni^{2+}/Mn^{2+} metal salt mixed solution. Calculate the size of the transfer filter paper (BP) according to the shrinkage, cut it into a circle, and immerse it in the above solution for 2 h. The obtained precursor material was dried at 60 °C for 12 h and carbonized in a tubular furnace at 800 °C in Ar/H_2 atmosphere for 2 h. The concentration of metal ions added in this work is 20, 40, 60, and 80 mM respectively, which are labeled as Sample 1, Sample 2, Sample 3, and Sample 4 in turn. For comparison, the synthesis method of CNFs is the same as above, but no metal salt solution is added to deionized water.

4.2. Materials characterization

The crystalline phase was identified by X-ray diffraction (XRD) on Rigaku D/max 2550 PC (CuKa). The structure and morphology research was performed with Zeiss Supra55 Scanning Electron Microscopy (SEM) and FEI TECNAIG2 F30 Transmission Electron Microscopy (TEM). Thermogravimetric (TG) analysis was recorded with a TG-209F1. The elemental composition and valence state are determined by X-ray photoelectron spectroscopy (XPS) (Kratos AXIS Ultra DLD XPS). The surface area and pore size distribution were determined using an ASAP 2020.

4.3. Synthesis of Li_2S_6/FCN-MO@CNFs

In the glove box, the sublimed sulfur and Li_2S are weighed at a molar ratio of 5:1, dissolved in 1,3-dioxolane/1,2-dimethoxyethane, and stirred at 60 °C for 48 h to obtain Li_2S_6 solution. Then, the solution is dropped into FCN-MO@CNFs to synthesize Li_2S_6/FCN-MO@CNFs. In this work, we adopted an S load of 1 mg cm^{-2}, which corresponds to a 0.2 M Li_2S_6 of 26 μL.

4.4. Electrochemical measurement

The electrochemical properties of Li_2S_6/FCN-MO@CNFs were tested by using CR2032 coin cells, which were assembled in an argon-filled glove box, where oxygen and moisture were both below 1 ppm. The cathode is Li_2S_6/FCN-MO@CNFs, the anode is Li, the separator is Celgard 2300, and the electrolyte is 50 μL 1.0 M bis-(trifluoromethane) sulfonamide lithium (LiTFSI) in DOL/DME (volume ratio = 1:1) with 0.2 M $LiNO_3$.

The galvanostatic charge/discharge tests were evaluated on the battery testing system (Neware) in the voltage range of 1.7 V–2.8 V and

a low-temperature galvanostatic discharge/charge test was recorded on the Land battery testing system. Electrochemical impedance spectroscopy (EIS) and cyclic voltammetry (CV) were measured on bio-logic VMP3 electrochemical workstation.

4.5. Assembly of symmetric cells

Two identical cathodes are used as the working electrode and the counter electrode. The active material is 26 μL 0.5 M Li_2S_6, and the electrode area is about 1 cm^{-2}. CV test was performed on the assembled symmetric battery at a certain scanning rate.

Declaration of Competing Interest

The authors declare that they have no known competing financial interests or personal relationships that could have appeared to influence the work reported in this paper.

Data availability

No data was used for the research described in the article.

Acknowledgement

The authors are thankful for the financial support from National Natural Science Foundation of China (No. 52172250 and No. 51972156).

Appendix A. Supplementary data

Supplementary data to this article can be found online at https://doi.org/10.1016/j.cej.2023.141445.

References

[1] X. Dong, Z. Guo, Z. Guo, Y. Wang, Y. Xia, Organic batteries operated at -70°C, Joule 2 (5) (2018) 902–913.
[2] D.A. Burns, A.E. Baumann, K.J. Bennett, J.C. Diaz, V.S. Thoi, Chemical sulfide tethering improves low-temperature Li-S battery cycling, ACS Appl. Mater. Interfaces 13 (43) (2021) 50862–50868.
[3] N. Zhang, T. Deng, S. Zhang, C. Wang, L. Chen, C. Wang, X. Fan, Critical Review on Low-Temperature Li-Ion/Metal Batteries, Adv. Mater. 34 (15) (2022) 2107899.
[4] A. Manthiram, Y. Fu, S.H. Chung, C. Zu, Y.S. Su, Rechargeable lithium-sulfur batteries, Chem. Rev. 114 (23) (2014) 11751–11787.
[5] A. Rosenman, E. Markevich, G. Salitra, D. Aurbach, A. Garsuch, F.F. Chesneau, Review on li-sulfur battery systems: an Integral Perspective, Adv. Energy Mater. 5 (16) (2015).
[6] Y. Li, Y. Zeng, Y. Chen, D. Luan, S. Gao, X.W.D. Lou, Mesoporous N-rich carbon with single-Ni atoms as a multifunctional sulfur host for Li-S Batteries, Angew. Chem. Int. Ed. (2022) e202212680.
[7] Z. Li, J. Zhang, B. Guan, D. Wang, L.M. Liu, X.W. Lou, A sulfur host based on titanium monoxide@carbon hollow spheres for advanced lithium-sulfur batteries, Nat. Commun. 7 (2016) 13065.
[8] Z. Li, J.T. Zhang, Y.M. Chen, J. Li, X.W. Lou, Pie-like electrode design for high-energy density lithium-sulfur batteries, Nat. Commun. 6 (2015) 8850.
[9] Y. Jiao, F. Wang, Y. Ma, S. Luo, Y. Li, A. Hu, M. He, F. Li, D. Chen, W. Chen, T. Lei, Y. Hu, Challenges and advances on low-temperature rechargeable lithium-sulfur batteries, Nano Res. (2022).
[10] Y.V. Mikhaylik, J.R. Akridge, Low temperature performance of Li/S batteries, J. Electrochem. Soc. 150 (3) (2003) A306.
[11] A. Gupta, A. Bhargav, J.P. Jones, R.V. Bugga, A. Manthiram, Influence of lithium polysulfide clustering on the kinetics of electrochemical conversion in lithium-sulfur batteries, Chem. Mater. 32 (5) (2020) 2070–2077.
[12] S.Y. Lang, R.J. Xiao, L. Gu, Y.G. Guo, R. Wen, L.J. Wan, Interfacial mechanism in lithium-sulfur batteries: how salts mediate the structure evolution and dynamics, J Am. Chem. Soc. 140 (26) (2018) 8147–8155.
[13] X. Wang, X. Zhao, C. Ma, Z. Yang, G. Chen, L. Wang, H. Yue, D. Zhang, Z. Sun, Electrospun carbon nanofibers with MnS sulfiphilic sites as efficient polysulfide barriers for high-performance wide-temperature-range Li-S batteries, J. Mater. Chem. A 8 (3) (2020) 1212–1220.
[14] C.-Y. Fan, Y.-P. Zheng, X.-H. Zhang, Y.-H. Shi, S.-Y. Liu, H.-C. Wang, X.-L. Wu, H.-Z. Sun, J.-P. Zhang, High-performance and low-temperature lithium-sulfur batteries: synergism of thermodynamic and kinetic regulation, Adv. Energy Mater. 8 (18) (2018).
[15] D.R. Deng, F. Xue, C.D. Bai, J. Lei, R. Yuan, M.S. Zheng, Q.F. Dong, Enhanced adsorptions to polysulfides on graphene-supported BN nanosheets with excellent Li-S battery performance in a wide temperature range, ACS Nano 12 (11) (2018) 11120–11129.
[16] Z. Zhou, G. Li, J. Zhang, Y. Zhao, Wide working temperature range rechargeable lithium-sulfur batteries: a critical review, Adv. Funct. Mater. 31 (50) (2021) 2107136.
[17] Z. Wang, X. Shen, S. Li, Y. Wu, T. Yang, J. Liu, T. Qian, C. Yan, Low-temperature Li-S batteries enabled by all amorphous conversion process of organosulfur cathode, J. Energy Chem. 64 (2022) 496–502.
[18] S. Zhu, Y. Wang, J. Jiang, X. Yan, D. Sun, Y. Jin, C. Nan, H. Munakata, K. Kanamura, Good low-temperature properties of nitrogen-enriched porous carbon as sulfur hosts for high-performance Li-S batteries, ACS Appl. Mater. Interfaces 8 (27) (2016) 17253–17259.
[19] P. Zeng, C. Liu, C. Cheng, C. Yuan, K. Dai, J. Mao, L. Zheng, J. Zhang, L.-Y. Chang, S.-C. Haw, T.-S. Chan, H. Lin, L. Zhang, Propelling polysulfide redox conversion by d-band modulation for high sulfur loading and low temperature lithium-sulfur batteries, J. Mater. Chem. A 9 (34) (2021) 18526–18536.
[20] Z. Yu, B. Wang, X. Liao, K. Zhao, Z. Yang, F. Xia, C. Sun, Z. Wang, C. Fan, J. Zhang, Y. Wang, Boosting polysulfide redox kinetics by graphene-supported Ni nanoparticles with carbon coating, Adv. Energy Mater. 10 (25) (2020).
[21] X.-S. Chen, Y. Gao, G.-R. Zhu, H.J. Chen, S.-C. Chen, X.-L. Wang, G. Wu, Y.-Z. Wang, Multifunctional interlayer with simultaneously capturing and catalytically converting polysulfides for boosting safety and performance of lithium-sulfur batteries at high-low temperatures, J. Energy Chem. 50 (2020) 248–259.
[22] Y. Wang, Y. Xu, S. Ma, R. Duan, Y. Zhao, Y. Zhang, Z. Liu, C. Li, Low temperature performance enhancement of high-safety Lithium-sulfur battery enabled by synergetic adsorption and catalysis, Electrochim. Acta 353 (2020).
[23] N. Gao, Y. Zhang, C. Chen, B. Li, W. Li, H. Lu, L. Yu, S. Zheng, B. Wang, Low-temperature Li-S battery enabled by CoFe bimetallic catalysts, J. Mater. Chem. A 10 (15) (2022) 8378–8389.
[24] X. Pang, H. Geng, S. Dong, B. An, S. Zheng, B. Wang, Medium-entropy-alloy feconi enables lithium-sulfur batteries with superb low-temperature performance, Small (2022) e2205525.
[25] P. Charvin, S. Abanades, F. Lemort, G. Flamant, Hydrogen production by three-step solar thermochemical cycles using hydroxides and metal oxide systems, Energy Fuels 21 (5) (2007) 2919–2928.
[26] M.A. Langell, C.W. Hutchings, G.A. Carson, M.H. Nassir, High resolution electron energy loss spectroscopy of MnO(100) and oxidized MnO(100), J. Vac. Sci. Technol., A: Vacuum, Surfaces, Films 14 (3) (1996) 1656–1661.